Ion dynamics in ultrafast laser ablation of copper target

Xiaochang Ni (倪晓昌)[1*], Anoop K.K.[2], Mario Bianco[2], Salvatore Amoruso[2], Xuan Wang (王 宣)[1,2], Tong Li (李 彤)[1], Minglie Hu (胡明列)[3], and Zhenming Song (宋振明)[4]

[1]*School of Electronic Engineering, Tianjin University of Technology and Education, Tianjin 300222, China*

[2]*CNR-SPIN and Dipartimento di Fisica, Università degli Studi di Napoli Federico II, Complesso Universitario Monte S. Angelo, Via Cintia, Napoli 80126, Italy*

[3]*Ultrafast Laser Lab, Key Laboratory of Opto-electronic Information Technology, Ministry of Education (Tianjin University), Tianjin 300072, China*

[4]*Department and Institute of Physics, School of Science, Tianjin Polytechnic University, Tianjin 300387, China*

[*]*Corresponding author: nixiaochang@tju.edu.cn*

Received July 10, 2013; accepted June 28, 2013; posted online August 30, 2013

We investigate the angular distribution and average kinetic energy of ions produced during ultrafast laser ablation (ULA) of a copper target in high vacuum. Laser produced plasma (LPP) is induced by irradiating the target with Ti:Sapphire laser pulses of ∼50 fs and 800 nm at an angle of incidence of 45°. An ion probe is moved along a circular path around the ablation spot, thereby allowing characterization of the time-of-flight (TOF) of ions at different angles relative to the normal target. The angular distribution of the ion flux is well-described by an adiabatic and isentropic expansion model of a plume produced by solid-target laser ablation (LA). The angular width of the ion flux becomes narrower with increasing laser fluence. Moreover, the ion average kinetic energy is forward-peaked and shows a stronger dependence on the laser pulse fluence than on the ion flux. Such results can be ascribed to space charge effects that occur during the early stages of LPP formation.

OCIS codes: 320.2250, 320.7085, 320.7120, 350.5400.
doi: 10.3788/COL201311.093201.

Laser ablation (LA) and laser produced plasmas (LPP) are interesting research topics because of their fundamental properties and use in a number of applications[1,2]. While the use of laser pulses with nanosecond (ns) durations is common, the development of intense femtosecond (fs) laser sources based on chirped pulse amplification (CPA) has resulted in several investigations on this new regime, and many applications have progressively shifted toward fs pulses[3,4]. Ultrafast LA (ULA) of solid targets and the resulting LPP differ significantly between fs and ns laser sources. In fs laser interaction with a metallic target, the time available for heat conduction is of the order of the electron-ion relaxation time, which is typically 1–10 ps. The hydrodynamic motion of the heated material begins on a similar time scale. Thus, in contrast to ns LA, ULA using fs lasers results in laser pulses that do not interact with the nascent LPP and complete absorption of the laser pulse energy into the target with a consequent reduction of the fluence threshold.

Previous studies on the material blow off produced during ULA show that ULA comprises two main components: a rapidly moving population of atoms and ions and a cloud of nanoparticles expanding at a lower velocity[5−8]. The characteristic properties of these atom and ion populations include angular distribution and kinetic energy, both of which depend on the target properties, laser beam characteristics (e.g., wavelength, pulse duration, spot size, etc.)[5−10], and particle layer thickness at the beginning of expansion[11,12]. Many of the studies on ULA are based on the imaging and spectroscopy of the produced plumes[5−9], although several reports on ion plume characterization with Langmuir probes or energy analyzers have been published[11−14]. In many of these reports, measurements were made only along the direction close to the target normal surface. Ion probes are used to investigate the angular distribution of the ion flux and kinetic energy in ULA of metallic targets using different laser sources, e.g., Nd:glass laser systems (∼250 fs at 527 nm)[11] and XeF lasers (∼500 fs at 248 nm)[12].

We report the angular properties of ions in a LPP obtained by ULA of a copper target using a Ti:Sapphire CPA system with ∼50 fs pulses at 800 nm and pulse intensities ranging from 3×10^{13} to 3×10^{14} W/cm^2 in a high-vacuum environment. We observe the presence of different components in the ion flux, the kinetic energies of which depend on the angle off the normal to the target surface. The ion plume is of finite angular width and evidently does not correspond to a nearly unidirectional flow along the target normal predicted by some ULA models[14]. The ion plume is well-described by predictions of the adiabatic and isentropic plume expansion model of Anisimov *et al.*[15,16], which is originally developed for the expansion of a neutral cloud of particles and has been successfully applied to the description of the angular distributions of particles generated in LA with ns and fs pulses[11,12,17,18].

A schematic of the experimental setup used in the current investigation is shown in Fig. 1. The laser pulses are provided by a Ti:Sapphire system (Legend, Coherent, USA), and variations in the energy of the laser pulse are achieved using a system based on a half-waveplate and a polarizer. The repetition rate of laser pulses hitting the target surface is reduced to 33 Hz, and the laser beam hits a 1-mm thick, 20×20 (mm) copper target (purity 99.99+%, supplied by GoodFellow). The target is posi-

tioned at the center of a vacuum chamber, ($\leqslant 10^{-6}$ mbar) and rotated to avoid local drilling. The duration required for the laser pulse to reach the target surface, as measured by a single-shot background free autocorrelation technique, is ~50 fs. The laser beam is focused at an angle of incidence of 45° onto the target surface using a plano-convex lens. The average pulse fluence F may be obtained using the relation E/S, where E is the incident laser energy and S is the area on the target estimated by measurement of the laser impact region as a function of the laser pulse energy ($S = 1.4 \times 10^{-4}$ cm^2)[19]. The ion probe is moved along a circular path in the $z - x$ plane (Fig. 1(b)). Angular measurements are made by varying the angle θ with respect to the target normal in the range of –90°–+90° to determine whether or not the laser beam incidence at 45° influences the hemispherical characteristics of the ion plume.

Following Doggett *et al.*[17], a planar ion probe facing the plasma flow was used for this investigation. The ion probe area was 2.5×5.0 (mm), and the distance between the probe and the target surface was 32 mm. The circuit diagram employed to bias the probe and register the collected ion current is schematically shown in Fig. 2(a). The bias voltage (V_{cc}) was maintained using a 1-μF capacitor, and the collected ion current was determined by recording the voltage signal across a 50-Ω load resistor with a digital oscilloscope. Prior to the experiments, the area of the collected ion signal was measured as a function of the bias voltage to determine the ion saturation region[17], as shown in Fig. 2(b). A negative bias voltage on the probe allowed the collection of positive ions. When the voltage was sufficiently high to prevent electrons with the highest thermal energies in the plasma from reaching the probe, the collected charge became saturated at a V_{cc} lower than approximately –15 V. The ion probe was biased at a constant working voltage within the saturation region, i.e., at $V_{cc} = -20$ V, during measurement.

The current signal provides an ion time-of-flight (TOF) signal that is proportional to both ion density, n_i, and ion flow velocity, u_i, through the following relationship:

$$I(t) = eAn_i(t)u_i(t), \quad (1)$$

where e is the electron charge, A is the probe collecting area, and t is the TOF measured relative to the arrival of the laser pulse. The zero time for the TOF measurement was provided by a fast photodiode that collects the laser light reflected off the target surface. Ion TOF profiles were recorded as a function of the probe angle θ for

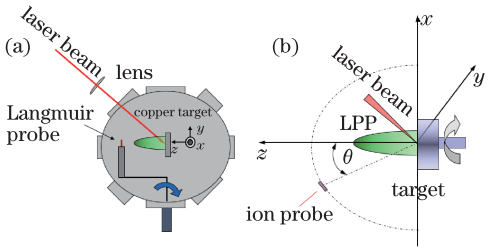

Fig. 1. (Color online) (a) Schematic of the experimental setup. The target is located in a high-vacuum chamber and the LPP is analyzed with a Langmuir probe moved along a circular path in the $z-x$ plane. (b) Sketch of the target, LPP, and ion probe positioning used in the experiment.

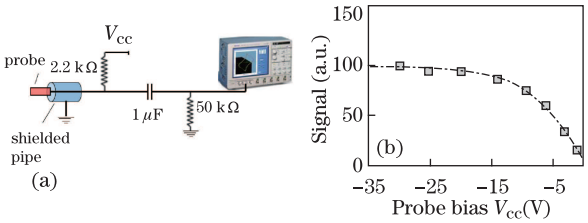

Fig. 2. (Color online) (a) Schematic diagram of the ion probe circuit. (b) Integrated intensity of the ion flux collected from the probe area versus bias-voltage V_{cc} showing the occurrence of the ion saturation region for V_{cc} lower than approximately –15 V.

different values of the laser pulse fluence F. Each profile was acquired from an average of over 16 laser shots.

Figure 3 shows typical ion TOF profiles recorded at various angles θ and a laser fluence F=10.7 J/cm^2. We observe the following: a) the signal intensity is largest along the normal ($\theta = 0°$) and progressively decreases with increasing angle, and b) the TOF profile leading edge moves toward longer TOF values as θ increases. These features suggest the presence of faster ions along the target normal. Similar behaviors are observed at lower fluence values. The inset in Fig. 3 shows an increase in ion TOF profiles recorded at larger angles, which indicates the presence of various components. Weaker features at TOF values below ~0.3 μs are due to residual low-Z contaminants[20,21], as confirmed by firing a number of single laser shots at the same position on a stationary target.

After the first shot, an intense peak with the same TOF value is observed, but the amplitude decreases when the next shots are fired, eventually reaching values comparable with those in Fig. 3. Given a rotating target with a repetition rate of several tens of Hz, appropriate conditioning of the target surface with a series of laser shots results in the negligible contribution of contaminants to the ablated plume species, which is in agreement with results of previous studies using plume spectroscopy techniques[22]. Signals obtained at very early TOFs decrease to values comparable with those observed for a stationary target after a number of laser shots are fired. All measurements were obtained after appropriate target conditioning/cleaning procedures. The contribution of low-Z contaminants to the overall ion TOF signal is 0.1%, which is inconsistent with the significant contribution of low-Z species present in the target considering its high purity. The presence of the low-Z peak can be explained by considering the diffusion of surface contaminants from the surrounding area into the cleaned laser spot, as reported by Williams *et al.*[21] under typical LA conditions. Note that the high quality of vacuum chamber used in our study reduces this contribution to nearly negligible levels[22].

With increasing duration of delays, two other features are observed in the ion TOF signals (indicated as peaks 1 and 2 in the inset in Fig. 3), further suggesting the presence of different components aside from the contaminant peak. For angles close to the target normal, two components are present in the form of a peak at a TOF of ~0.5 μs and a shoulder at a TOF of ~1.5–2.0 μs. The presence of more than one component in the ion plume produced in the ULA experiments of metallic targets

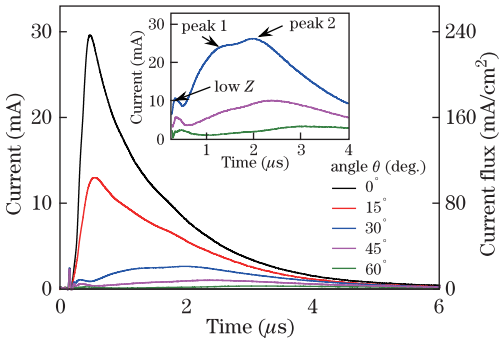

Fig. 3. (Color online) TOF ion signals for various angles θ relative to the target normal. Inset: Magnified image of the TOF ion profiles at selected angles showing the presence of various components.

has been previously reported by other authors[13,23–25]. Zhang *et al.*[13] observed two distinct ion populations in the energy spectrum of plasma plumes produced during ULA of Al and Ni targets with ∼80–100-fs Ti:Sapphire laser pulses, as measured by an ion energy analyzer ∼1 m from the target surface. The presence of differently charged ionization states of up to +3 has been reported for Al. Comparison with the ion probe signal recorded ∼10 cm from the target surface for Ni indicates overall agreement among ion kinetic energies. However, a significant overlap of the two components is recorded by the ion energy analyzer. The same authors attribute the more-energetic ion population to a combination of ambipolar field effects, Coulomb explosions, and nonlinear ponderomotive forces and the less-energetic ion population to a hydrodynamic component with ns pulses under similar conditions[13]. Double peak ion TOF profiles have also reported by Ye *et al.*[23,24] during ULA of metals (Ti, Cu, Au) with ∼80–100-fs Ti:Sapphire laser pulses.

Double peak ion structures have been reported by Verhoff *et al.*[25] using a Faraday cup detector positioned ∼14 cm from the target surface during ULA of Al with ∼40 fs Ti:Sapphire laser pulses. Simultaneous measurements with a 6-ns pulse from a Nd:YAG laser do not reveal energetic components. Instead, other experiments with visible (∼250 fs, 527 nm), and ultraviolet (∼500 fs, 248 nm) fs laser pulses did not reveal the presence of a significant energetic component[11,12]. The same experimental setup is used in our previous experiments with laser pulses of ∼250 fs at 527 nm. Thus, any influence exerted by the experimental apparatus can be excluded. The pulse durations and fluences used in the two previous studies are very different, resulting in diverse levels of interaction. The average pulse intensity, $I_{\rm L}$, is investigated in the interval $\sim(0.3–2)\times10^{12}$ W/cm^2 at 527 nm in a previous study, whereas $I_{\rm L}$ varies in the range $\sim(0.3–2)\times10^{14}$ W/cm^2 in the present study. This result suggests that the generation of fast ions depends on mechanisms related to laser pulse intensity.

A mechanism that may account for the production of energetic ions in LA is the rapid formation and expansion of a space-charge layer of electrons that creates a time-dependent ambipolar field, as discussed previously by Zhang *et al.*[26,27] in LA studies using fs Ti:Sapphire laser pulses at intensities comparable with those used in the present study. This layer forms because energetic electrons escape at the edge of plasma at distances comparable with the Debye plasma length[28]. The electrons set up a space charge layer, which consequently accelerates a fraction of the plasma ions. By contrast, the core of the plume, which is neutral, undergoes a hydrodynamic expansion away from the target. Such a mechanism results in the double-component distribution observed in the ion TOF profiles. The high-energy component contains hot electrons and accelerated ions, whereas the second peak comprises thermalized ions and electrons expanding in vacuum. This mechanism is fairly effective in accelerating energetic ions at a narrow angle along the normal to the target surface, as suggested by the predominance of signals for $\theta = 0°$ and $\theta = 15°$ in Fig. 3. At larger angles, signals progressively become lower than the second slower component.

The ion TOF profiles are integrated to investigate the angular dependence of the ion charge flux collected by the probe. As the two ion peaks are not separated easily, the overall signal is evaluated, except for the very minor contribution of low-Z contaminants at early TOF. The angular variation of the charge flux is shown in Fig. 4(a). The curves are symmetrical relative to the target normal, but the maximum flux does not always occur at $\theta = 0°$ because of the limited mechanical precision of the probe holder. The charge flux is fitted with the angular distribution $F(\theta)$ predicted by the expansion model of Anisimov *et al.*[15,16,20] for collection on a hemispherical surface:

$$F(\theta) = F_0[1 + \tan^2(\theta)]^{3/2}[1 + k_{zx}^2 \tan^2(\theta)]^{-3/2}, \quad (2)$$

where F_0 is the maximum flux value and k_{zx} is the asymptotic value of the longitudinal-to-transverse axes ratio of the semi-ellipsoidal shaped plume in the zx plane (see Fig. 1(b)). The parameter k_{zx} is related to the plume aspect ratio, and larger values correspond to a more forward-peaked expansion. In the fitting procedure, the angle corresponding to the maximum intensity is left as a parameter that always coincides with the nominal $\theta = 0°$ position by a few degrees.

Figure 4(b) reports the dependence of k_{zx} on F. The increase in the k_{zx} value with F indicates a more forward-peaked ion plume at larger fluence, which is in agreement with previous reports[20]. The values of the corresponding angular width $\Delta\theta$ (FWHM) are shown in Fig. 4(b). An angular width in the order of 20° is consistent with that reported for an Al LPP produced by ∼40-fs Ti:Sapphire laser pulses[25]. In other reports[11,29], narrower ion plumes are observed. This width difference is due to our use of smaller laser beam spot sizes on the target in our experiment, resulting in larger LPP angular widths. These results are in agreement with model predictions[15,16,20]. The angular distribution of the LPP ions is well-described by the Anisimov model using realistic parameters related to the specific experimental conditions.

From the ion TOF signals, the ion average kinetic energy ⟨KE⟩ is calculated, and its angular variation was derived. ⟨KE⟩ is obtained as

$$\langle \mathrm{KE} \rangle = \frac{1}{2} m_{\mathrm{Cu}^+} \langle u^2 \rangle, \quad (3)$$

where $\langle u^2 \rangle$ is the ion mean square velocity evaluated as

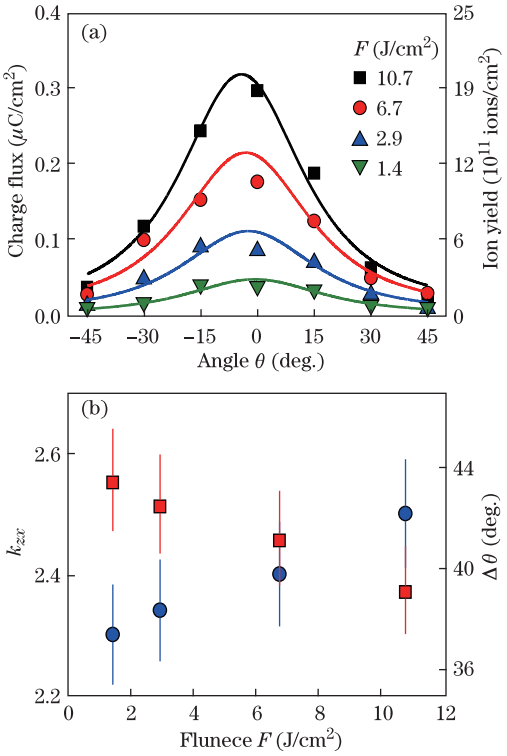

Fig. 4. (Color online) (a) Angular variations of the collected charge flux for different values of laser pulse fluence F. (b) Aspect ratio, k_{zx} (blue dots), and corresponding angular widths (FWHM) $\Delta\theta$ as a function of laser pulse fluence F.

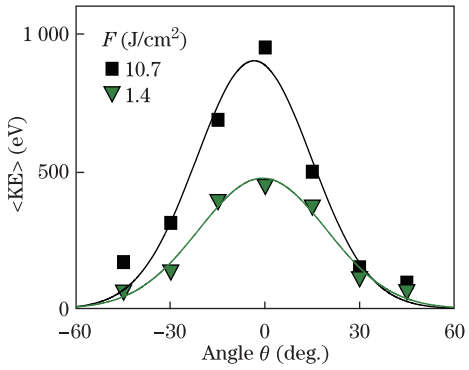

Fig. 5. (Color online) Angular variation of the ion average kinetic energy $\langle$KE$\rangle$ for two different values of laser pulse fluence F. The curves are Gaussian fits to the experimental data.

$$\langle u^2\rangle = \frac{\int \left(\frac{L_\mathrm{p}}{t}\right)^2 I(t)\mathrm{d}t}{\int I(t)\mathrm{d}t}, \qquad (4)$$

and L_p is the target-to-probe distance[30].

The angular variation of $\langle$KE$\rangle$ for two values of F is reported in Fig. 5. In both fluence conditions, the average ion energy in the direction normal to the target is greatest, indicating a forward-peaked distribution of $\langle$KE$\rangle$ that reaches energy values of several hundred eV. Moreover, from 0° to ~30°, $\langle$KE$\rangle$ decreases by a factor 6 at 10.7 J/cm^2 and by a factor of 3 at 1.4 J/cm^2. These findings indicate that the majority of the ions are concentrated in a rather narrow cone angle relative to the target normal. In particular, the LPP ion plume has angular widths (FWHM) of ~36° at 10.7 J/cm^2 and ~41° at 1.4 J/cm^2, corresponding to the broadening of the distribution as the fluence decreases. These values are consistent with those observed for LPPs produced by ~40-fs Ti:Sapphire laser pulses irradiating an Al target[25]. The larger effect of F on the forward-focusing of $\langle$KE$\rangle$ relative to the ion flux is consistent with more electrons forming the space-charge layer at higher laser intensities to result in stronger acceleration during the early stages of ULA in the forward direction.

In conclusion, we study the dynamics of ions in a LPP formed during ULA of a copper target in high vacuum using fast ion probe diagnostics. Ion TOF signals show the presence of a more-energetic component, which follows either fs or ns LA, as well as a hydrodynamic component typically observed in LPPs. This faster component has previously been reported under experimental conditions similar to those used in this study and is characterized as a space charge effect that accelerates some of the ions formed during early stages of ULA. The angular distribution of ions can be analyzed in terms of the general model of Anisimov *et al.*[15,16], which quantifies the aspect ratio of the LPP ions. The angular distribution of the ion flux and average kinetic energy are studied at various laser fluences, and a progressive narrowing of the distribution is observed at increasing fluences. In particular, from 0° to ~30°, reductions in the ion flux occur in the interval from 3.5 to 4.1, and the corresponding change in $\langle$KE$\rangle$ varies from ~3 at 1.4 J/cm^2 to 6 at 10.7 J/cm^2. These findings suggest the significant effect of F on the forward-focusing of $\langle$KE$\rangle$ relative to the ion flux. The results promote an improved understanding of the mechanisms of plasma formation in ULA and help optimize LPP parameters in various applications.

This work was supported by the China National Scholarship Fund, the Executive Programme Italy-China for the years 2010–2012 (No. CN10M02), the National Natural Science Foundation of China (No. 11104201), and the Key Laboratory of Opto-electronic Information Technology, Ministry of Education (Tianjin University) Open Fund and the European Union Seventh Framework Programme (FP7/2007–2013) (No. 264098-MAMA). The authors would like to thank Dr. D. Paparo of CNR-SPIN for assisting with the laser system and Prof. R. Bruzzese for his suggestions and comments.

References

1. C. R. Phypps, *Laser Ablation and Its Applications* (Springer, New York, 2007).
2. X. Ni, C. Wang, L. Yang, J. Li, L. Chai, W. Jia, R. Zhang, and Z. Zhang, Appl. Surf. Sci. **253,** 1616 (2006).
3. Y. Ju, C. Liu, Y. Liao, Y. Liu, L. Zhang, Y. Shen, D. Chen, and Y. Cheng, Chin. Opt. Lett. **11,** 072201 (2013).
4. Z. Song, S. Wang, Y. Sun, K. Shang and X. Ni, Chin. Opt. Lett. **10,** S23201 (2012).
5. S. Amoruso, G. Ausanio, R. Bruzzese, M. Vitiello, and X. Wang, Phys. Rev. B **71,** 033406 (2005).
6. S. Noël, J. Hermann, and T. Itina, Appl. Surf. Sci. **253,** 6310 (2007).
7. J. Perrière, C. Boulmer-Leborgne, R. Benzerga, and S.

Tricot, J. Phys. D Appl. Phys. **40,** 7069 (2007).
8. S. Amoruso, R. Bruzzese, X. Wang, N. N. Nedialkov, and P. A. Atanasov, J. Phys. D Appl. Phys. **40,** 331 (2007).
9. S. Amoruso, N. N. Nedyalkov, X. Wang, G. Ausanio, R. Bruzzese, and P. A. Atanasov, J. Appl. Phys. **110,** 124303 (2011).
10. G. O. Williams, S. Favre, and G. M. O'Connor, Appl. Phys. Lett. **94,** 101503 (2009).
11. T. Donnelly, J. G. Lunney, S. Amoruso, R. Bruzzese, X. Wang, and X. Ni, Appl. Phys. A **100,** 569 (2010).
12. B. Toftmann, B. Doggett, C. Budtz-Jørgensen, J. Schou, and J. G. Lunney, J. Appl. Phys. **113,** 083304 (2013).
13. Z. Zhang, P. A. VanRompay, J. A. Nees, and P. P. Pronko, J. Appl. Phys. **92,** 2867 (2002).
14. A. M. Komashko, M. D. Feit, and A. M. Rubenchik, Proc. SPIE **3935,** 97 (2000).
15. S. I. Anisimov, D. Bäuerle, and B. S. Luk'yanchuk, Phys. Rev. B **48,** 12076 (1993).
16. S. I. Anisimov, B. S. Luk'yanchuk, and A. Luches, Appl. Surf. Sci. **96–98,** 24 (1996).
17. B. Doggett and J. G. Lunney, J. Appl. Phys. **105,** 033306 (2009).
18. B. Toftmann, J. Schou, and J. G. Lunney, Phys. Rev. B **67,** 104101 (2003).
19. J. M. Liu, Opt. Lett. **7,** 196 (1982).
20. T. Donnelly, J. G. Lunney, S. Amoruso, R. Bruzzese, X. Wang, and X. Ni, J. Appl. Phys. **108,** 043309 (2010).
21. G. O. Williams, G. M. O'Connor, P. T. Mannion, and T. J. Glynn, Appl. Surf. Sci. **254,** 5921 (2008).
22. X. Wang, S. Amoruso, and J. Xia, Appl. Surf. Sci. **255,** 5211 (2009).
23. M. Q. Ye and C. P. Grigoropoulos, J. Appl. Phys. **89,** 5183 (2001).
24. S. Amoruso, X. Wang, C. Altucci, C. de Lisio, M. Armenante, R. Bruzzese, and R. Velotta, Appl. Phys. Lett. **77,** 3728 (2000).
25. B. Verhoff, S. S. Harilal, and A. Hassanein, J. Appl. Phys. **111,** 123304 (2012).
26. Z. Zhang, P. A. Van Rompay, J. A. Nees, C. A. Stewart, X. P. Pan, L. Fu, and P. P. Pronko, Proc. SPIE **3935,** 86 (2000).
27. S. Amoruso, X. Wang, C. Altucci, C. de Lisio, M. Armenante, R. Bruzzese, N. Spinelli, and R. Velotta, Appl. Surf. Sci. **186,** 358 (2002).
28. R. P. van Ingen, J. Appl. Phys. **76,** 8055 (1994).
29. P. T. Mannion, S. Favre, C. Mullan, D. S. Ivanov, G. M. O'Connor, T. J. Glynn, B. Doggett, and J. G. Lunney, J. Phys. Conf. Ser. **59,** 753 (2007).
30. T. Donnelly, B. Doggett, and J. G. Lunney, Appl. Surf. Sci. **252,** 4445 (2006).